Loop-Fed Planar Inverted-L Antennas (PILAs) for Omnidirectional UHF on-Metal Tag Design

Yong-Hong Lee, *Member, IEEE*, Eng-Hock Lim, *Senior Member, IEEE*, Fwee-Leong Bong, and Boon-Kuan Chung

***Abstract*— A new type of tag antenna, which is made by placing four identical planar inverted-L antennas (PILAs) in rotational symmetry constellation, is proposed for designing a miniature on-metal tag antenna. It shows good omnidirectional characteristics in the azimuth plane. In the design, the directive radiation beams of the respective PILAs are tactfully combined to form a stable omnidirectional pattern. The proposed tag is compact with a small size of 40 mm × 40 mm × 1.6 mm (0.122 λ × 0.122 λ × 0.005 λ). Here, all the PILAs are inductively excited by a circular loop, which also introduces additional reactance for improving the impedance matching. The proposed tag antenna is able to achieve a stable read distance of 5.9 m on metal in the azimuth plane when it is tested using equivalent isotropic radiated power of 4 W. The operating frequency of the tag is stable and it is not affected much by changes in the backing metal.**

***Index Terms*— Omnidirectional, on-metal, UHF radio frequency identification (RFID) tag.**

I. Introduction

THE demand for the UHF radio frequency identification (RFID) tagging technology has been rapidly growing over the past decades and its applications can now be found in many sectors such as retail, logistics, transportation, and inventory management. The UHF RFID tags, which are used as identifiers for their tagged objects, are required to be small in size, low in profile, long in read distance, and performing stably on all platforms, particularly on metal. This is because the image currents caused by the conducting surface can significantly jeopardize the radiation performances of a tag antenna [1]. In many practical applications, omnidirectional tags are in great demand as they are able to provide spatial coverage in all directions in the azimuth plane. Among all, dipole and monopole are the two most common antennas that are able to provide good omnidirectional characteristics. The strip dipole with a split-ring resonator (SRR) in [2] has good omnidirectional radiation patterns in the vertical plane. However, such planar-type dipolar tag antenna loses its omnidirectional characteristics and it becomes a directional antenna when it is tagged on metal surface [3], [4]. Similar effect is also observed in the planar monopolar tag antenna in [5]. Although a monopole can be easily built vertically [6] on the metal plane to radiate omnidirectionally, this is not practical as the antenna profile is simply too high for designing a UHF RFID tag. In [7], four planar folded dipoles are employed for designing an omnidirectional antenna with gain fluctuation in the azimuth plane of less than 2 dB. However, again, the antenna profile is very high (∼27 mm). Also, the Alford loop antenna [8] and capacitive-loaded loop antenna [9] have been employed for designing various low-profile omnidirectional antennas that have a radiation pattern similar to that of the vertical dipole. Nevertheless, these antennas radiate only horizontally polarized waves, making them not suitable for designing on-metal tags. Due to the boundary condition, the horizontally polarized waves rapidly attenuate on metal surface [10]. In recent years, the patch and dielectric resonators have also been explored for designing various omnidirectional antennas. The patch antennas in [11] and [12] have employed multiple shorting vias/pins to generate dual-polarized or even circularly polarized omnidirectional radiation patterns. However, fabricating metallic vias/pins requires additional PCB processes, which are not economical for commercial purposes. Moreover, the omnidirectional characteristics of such antennas are usually very sensitive to changes of locations and dimensions of the shorting elements, making the tuning processes very tedious. A couple of omnidirectional antennas which are designed using the dielectric resonators can also be found in [13] and [14]. However, again, the resonators are high in profile and they are costly due to the use of high-dielectric-constant materials.

In this article, a low-profile omnidirectional tag antenna is proposed for on-metal applications. Four identical planar inverted-L antennas (PILAs), each of which is a directive antenna on its own [15], are closely placed in rotational symmetry manner so that their radiation patterns can be tactfully combined to form a good omnidirectional in the azimuth plane on metal. A circular feeding loop, which is used to excite all four PILAs simultaneously, is able to introduce additional reactance to the antenna for achieving conjugate match with the chip impedance. To the best of our knowledge, the proposed antenna structure here is the first planar omnidirectional patch-type tag antenna that is usable for on-metal applications. Being not only compact in size but

Manuscript received April 17, 2019; revised March 8, 2020; accepted March 29, 2020. Date of publication April 30, 2020; date of current version August 4, 2020. This work was supported by the Collaborative Research in Engineering, Science and Technology, Malaysia, through a targeted CREST Fund, under Grant T07C2-15. *(Corresponding author: Eng-Hock Lim.)*

Yong-Hong Lee, Eng-Hock Lim, and Boon-Kuan Chung are with the Electrical and Electronic Engineering Department, Universiti Tunku Abdul Rahman, Kajang 43000, Malaysia (e-mail: limeh@utar.edu.my).

Fwee-Leong Bong is with the Engineering and Built Environment Department, Tunku Abdul Rahman University College, Tanjong Bungah 11200, Malaysia.

Color versions of one or more of the figures in this article are available online at http://ieeexplore.ieee.org.

Digital Object Identifier 10.1109/TAP.2020.2990287

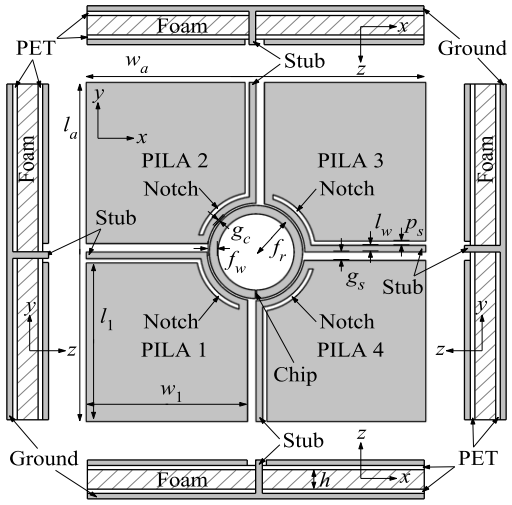

Fig. 1. Orthographic views of the antenna configuration.

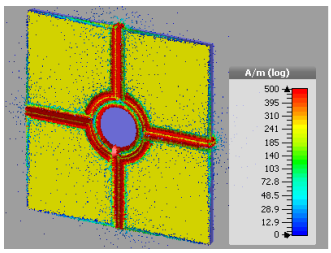

Fig. 2. Surface current distribution on the tag antenna at a resonant frequency of 915 MHz.

also low in profile, it will be shown later that our proposed tag antenna is vertically polarized and has good omnidirectional characteristics in the azimuth plane on metal. This article is organized as follows. In Section II, the antenna configuration is studied and an equivalent circuit is developed for analyzing the impedance characteristics of the tag antenna. The measurement setup is further elaborated in Section III. The input impedance, tag sensitivity, realized gain, and read patterns are presented in Section III. The performances of the tag antenna are also tested for several actual implementation scenarios.

II. Configuration and Equivalent Circuit

A. Antenna Structure Design

The proposed antenna comprises two conductive layers: four radiating patches that are placed in rotational symmetry constellation on the top surface and a metallic layer which functions as a ground plane underneath. The inlay is made by etching away a copper lamination ($t = 0.009$ mm) which was initially deposited on a flexible thin polyethylene terephthalate (PET, 50 μm) film. Then, it is wrapped around a piece of polyethylene foam substrate ($\varepsilon_r = 1.06$, $\tan\delta \sim 0.0001$) [16] which has a thickness of $h = 1.6$ mm. As can be deduced from [7], [9], [12], and [13], the proposed antenna structure needs four elementary resonators arranged in the form of a circular array for achieving good omnidirectional radiation pattern in the azimuth plane. This can be done by partitioning the antenna structure into four identical quadrants to accommodate the symmetric elements individually. Referring to Fig. 1, the PILAs (PILA 1, PILA 2, PILA 3, and PILA 4) on the top surface are all geometrically rotated (90°). This arrangement is able to improve the co-polarization level by having the cross-polarization radiations from the elementary resonators canceled out each other [17]. Referring to the same figure, each of the patches is etched with a long notch (p_s) along its right edge to carve out a long and thin inductive stub (l_w). The stub is to provide additional inductance for the PILA to resonate at 915 MHz. Each of the PILAs is shorted to the ground plane underneath through the inductive stub. Referring to Fig. 1 again, the PILAs in the circular array are placed in series around the circular loop and they are simultaneously excited through inductive coupling. The feeding loop, which is made of a concentric high-impedance line, is also introducing inductive reactance to the antenna impedance for achieving conjugate match with the large capacitance of the chip [18]. Therefore, this design does not require additional matching networks. A narrow gap on the loop is for accommodating the RFID microchip (Monza 5) [19]. Finally, the design parameters are optimized by using the genetic algorithm optimizer of the CST Microwave Studio. In the design process, a few parameters ($l_a = 40.00$ mm, $w_a = 40.00$ mm, and $h = 1.6$ mm) are first fixed, while others are obtained through optimization processes. By setting the antenna gain, power transmission coefficient, and magnetic coupling between the loop and the PILAs as the objective functions, the optimization processes will be halted automatically as soon as all the functions are met. After several iterations, the optimized values are found to be: $l_1 = 18.70$ mm, $l_w = 0.80$ mm, $w_1 = 19.00$ mm, $g_s = 1.00$ mm, $g_c = 0.25$ mm, $f_w = 1.00$ mm, $f_r = 5.00$ mm, and $p_s = 0.50$ mm.

In simulation, the tag antenna is placed at the center of a piece of 20 × 20 cm^2 aluminium plate as it is designed to be used for on-metal applications. The simulated surface current distribution is shown in Fig. 2. High current densities are found along the stubs that join the patches to the ground, showing that the stubs' width can be effectively used for tuning the impedance of the tag antenna. In addition, it is found that the feeding loop has successfully excited all the four PILAs, making them resonate in the same phase. To further verify this, the electric and magnetic field distributions are simulated and illustrated in Fig. 3. Owing to the low-profile structure, with reference to Fig. 3(a) and (b), four cavities are formed in between radiating patches and the ground plane. Due to the existence of the top (patches) and bottom (ground) metallic layers, the tangential electric fields must be zero in the cavities to satisfy the boundary condition, as shown in Fig. 3(a). The electric fields are found to be stronger around the edges of the patch. This is reasonable as the open edges are electrically open. It is also found that the electric field distribution of the proposed antenna is very similar to that radiated by a vertical dipole, which is vertically polarized. With reference to Fig. 3(b), transverse magnetic (TM) fields are formed inside the cavities. From the electric and magnetic field distributions, it can be concluded that all the PILAs are resonating at the TM mode, which is typical for patch-like resonators. The conventional mode annotation cannot be used

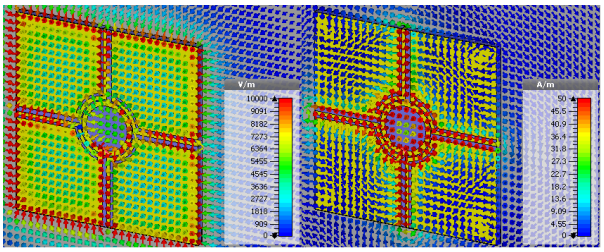

Fig. 3. (a) Electric field and (b) magnetic field distributions at resonance.

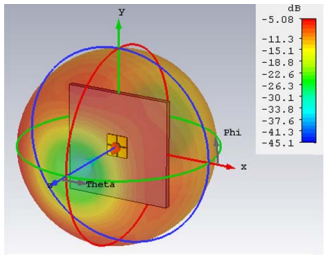

Fig. 4. 3-D simulated radiation pattern.

here as the patch size is electrically very small. Meanwhile, strong magnetic fields at the center show that good inductive coupling between the feeding loop and the PILAs has been achieved. The feeding loop in this design is electrically small and it has poor radiation efficiency. As a result, it is only able to function as an exciter and it does not contribute to the far-field radiation. With reference to Fig. 4, the tag antenna exhibits good omnidirectional characteristics in all directions in the azimuth plane, achieving a constant antenna gain of approximately -5.08 dBi when it is tagged on an aluminium plate. It is also found that the proposed tag antenna is able to achieve a radiation efficiency of $e_{cd} = 0.217$ at resonance, which is a reasonable value for an electrically small tag antenna [20].

To show the necessity to have four PILAs for designing the proposed omnidirectional tag antenna, the radiation patterns for the cases of one and two PILAs are also simulated and the results are shown in Figs. 5 and 6. As shown in Fig. 5, the achievable antenna gain is approximately -9 dBi when only PILA 1, 2, 3, or 4 is involved, with the main beam pointing in the direction of $\phi = 180°$, $90°$, $0°$, and $270°$, respectively. The maximum field point is $\theta = 47°$ due to the existence of the aluminium plate. With reference to Fig. 6, when the two PILAs are incorporated into the tag design, the beam coverage can be increased depending on the arrangement of the resonators. When the two PILAs are placed side by side, as shown in Fig. 6(a)–(d), the respective beamwidth is further broadened to cover a broader range annularly in the azimuth plane. As a result, the antenna gain has improved to approximately -6 dBi, seeing a 3 dB increase in the magnitude. This is not unusual and it can be explained by the array theory, which relates the antenna gain with the number of elements in the array. However, when the two PILAs are diagonally placed, as shown in Fig. 6(e) and (f), a nearly omnidirectional radiation pattern is obtainable. The field distribution is not even and the difference between the maximum and minimum gains

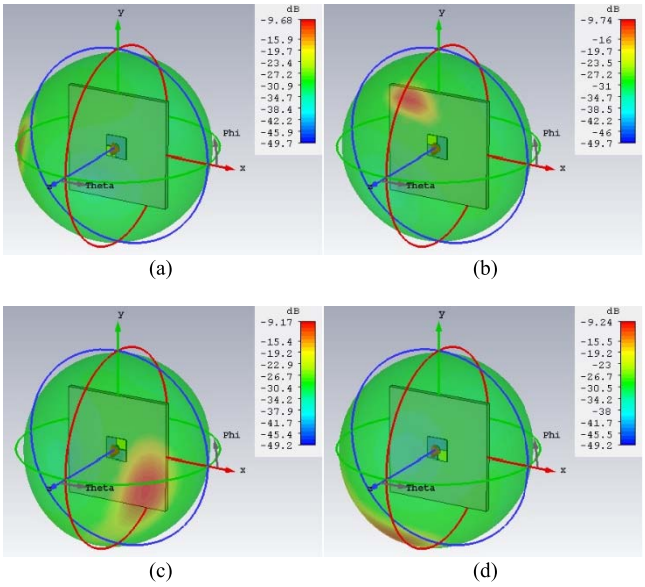

Fig. 5. 3-D simulated radiation patterns of (a) PILA 1, (b) PILA 2, (c) PILA 3, and (d) PILA 4.

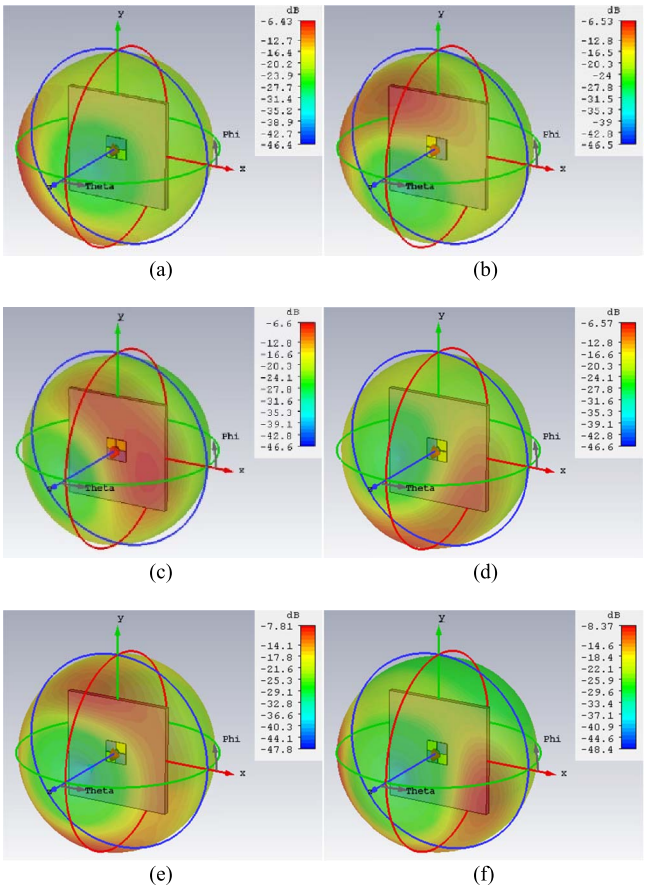

Fig. 6. 3-D simulated radiation patterns of (a) PILAs 1 and 4, (b) PILAs 1 and 2, (c) PILAs 2 and 3, (d) PILAs 3 and 4, (e) PILAs 1 and 3, and (f) PILAs 2 and 4.

is $\sim$1 dB. It shows that employing all four PILAs into the circular array arrangement is effective for achieving uniform field distribution in all the azimuth directions.

Subsequently, parametric analysis is performed in order to analyze the effects of the design parameters. The effects of

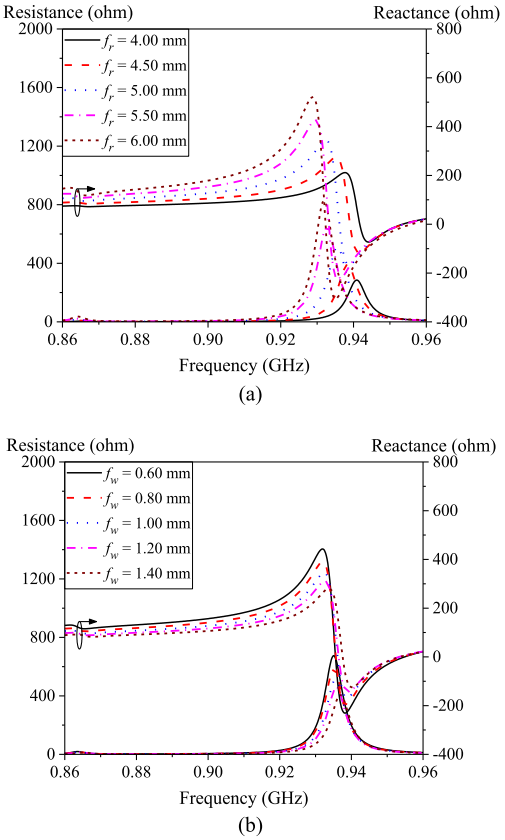

Fig. 7. Effects of changing the dimensions (a) f_r and (b) f_w of the feeding loop. Other parameters remain unchanged.

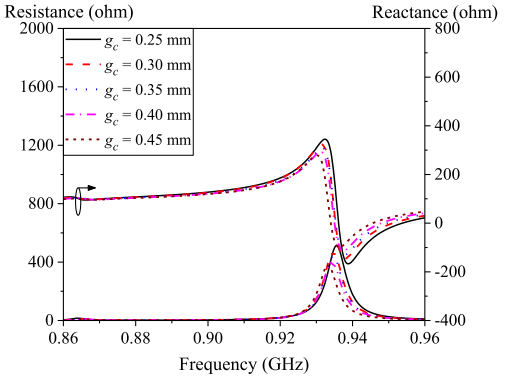

Fig. 8. Effect of varying the coupling gap between the feeding loop and the PILAs.

changing the dimensions of the feeding loop are first studied and the simulated results are shown in Fig. 7. Increasing the loop radius (f_r) and reducing the trace width (f_w) make the loop more inductive, causing the input reactance (X_{in}) to increase at the rate of 74.80 and 88.70 Ω/mm, respectively. It shows that changing the loop dimensions is useful for improving the impedance matching. The effect of the coupling gap (g_c) on the antenna impedance is also studied in Fig. 8. Changing g_c introduces small tuning sensitivity of $\partial f/\partial g_c =$ 15 MHz/mm, which is suitable for fine-tuning purpose.

Next, the effects of changing the dimensions of the four PILAs are studied and the simulated impedances are plotted in Fig. 9. As shown in Fig. 9(a), changing the stubs' width (l_w)

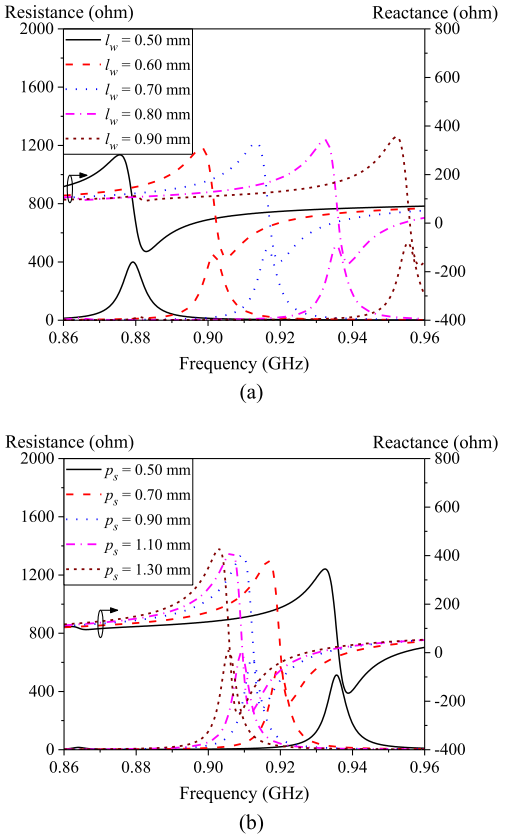

Fig. 9. Effects of changing the design parameters (a) l_w and (b) p_s of the PILAs.

allows X_{in} to be tuned in a wider range, making this parameter useful for coarse-tuning the resonant frequency from 862 to 934 MHz. Similar effect is also observed in Fig. 9(b) when the notches' width (p_s) is increased.

B. Equivalent Circuit Model

Next, the equivalent circuit model of the proposed tag antenna is derived for analyzing its impedance characteristics. With reference to Fig. 10(a), the circular loop is magnetically coupled to all the four PILAs concurrently and its equivalence can be modeled as a series of lumped resistance and inductance that are connected in parallel to a shunt capacitance [21]. The parasitic capacitance (C_f), which is attributed to the input port in the small circular loop, is trivial and as a result, it is neglected in the subsequent derivations. The loss and radiation resistances [22] of the feeding loop can be expressed as the first and second terms in (1), respectively, and the total resistance is calculated to be $R_f = 0.139\ \Omega$

$$R_f = \frac{\pi f_r}{(f_w + t)}\sqrt{\pi f \rho \mu_0} + 20(2\pi)^4\left(\frac{\pi f_r^2}{\lambda^2}\right)^2 \tag{1}$$

where the copper resistivity is $\rho = 1.72 \times 10^{-8}\Omega\cdot$m. The equivalent inductance of the feeding loop (L_f) is calculated to be 14.967 nH by using the approximation equation given as follows [23]:

$$L_f = \mu_0 f_r\left[\ln\left(\frac{16 f_r}{f_w}\right) - 2\right]. \tag{2}$$

PILAs, which are also the elementary radiators of the proposed antenna, can be modeled as lumped elements R, C, and L cascaded in series. Referring to Fig. 10(a) again, the equivalent inductance (L) of each PILA is modeled as three partial inductances in order to facilitate the subsequent derivations. In the case of PILA 1, for example, the partial inductances are contributed by the radiating patch (L_{r1}), the arc (L_{a1}), and the straight-line segment (L_{s1}) of the inductive stub, and they can be approximated by using (3)–(5) [24], [25]. The total inductance of PILA 1 (L_1) ends up to be 15.469 nH after adding up the partial inductances

$$L_{r1} = \frac{\mu_0 w_1}{2\pi}\left[\ln\left(\frac{2w_1}{l_1+t}\right)+\frac{1}{2}+\frac{2}{9}\left(\frac{l_1+t}{w_1}\right)\right] \tag{3}$$

$$L_{a1} = \frac{\mu_0 x_a}{2\pi}\left[\ln\left(\frac{l_w+p_s}{l_w+t}\right)+\frac{3}{2}\right] \tag{4}$$

$$L_{s1} = \frac{\mu_0 (x_s+h) K(k')}{4K(k)} \tag{5}$$

where $x_s = 13.92$ mm and $x_a = 8.55$ mm are the lengths of the straight and arc segments of the inductive stub, respectively. $K(k) = 1.658$ and $K(k') = 2.266$ are the complete elliptic integral of the first kind with $k = (l_w - \delta)/(l_w + 2p_s + \delta) = 0.443$, $k' = \sqrt{(1-k^2)} = 0.897$, and the skin depth is $\delta = 2.18 \times 10^{-6}$ m. The resistance of the PILA 1 (R_1), which is the sum of the loss resistance (R_{loss}) and the radiation resistance (R_{rad}) defined in (6) and (7), is approximated to be $R_1 = 0.410\ \Omega$ [26], [27]

$$R_{\text{loss}} = \frac{\rho K_c s_1}{l_w t\left(1-\exp\left(-\frac{2\delta}{t}\left(1+\frac{t}{l_w}\right)\right)\right)} \tag{6}$$

$$R_{\text{rad}} = \frac{30\beta^2(2h)^2}{\cos^2\beta s}\left[\begin{array}{l}\frac{1}{2}\left(\cos^2\beta s+\sin^2\beta s_1+\cos^2\beta s_2\right)\\ -\cos\beta s\cos\beta s_2\dfrac{\sin\beta s_1}{\beta s_1}\end{array}\right] \tag{7}$$

where the current crowding factor is $K_c = 1.81$, $\beta = 2\pi/\lambda$, $s_1 = x_a + x_s + h$, $s_2 = l_1 + w_1$, and $s = s_1 + s_2$. Meanwhile, the capacitive loading ($C_1 = 1.870$ pF) between the radiating patch and the ground plane underneath can be determined by using the following:

$$C_1 = \frac{\varepsilon_0 \varepsilon_r A_p}{h} \tag{8}$$

where $A_p = 0.000325\ \text{m}^2$ is the effective area of the radiating patch.

As illustrated in Fig. 3(b), strong magnetic flux at the center shows that coupling only involves the feeding loop and the arc segments of the PILAs. As a result, a simplified circuitry, as shown in Fig. 10(b), can be used for analyzing the mutual coupling. This circuit resembles a conventional multiwinding transformer [28], where the voltage and current on each secondary winding (PILA) are induced (M_{f1}, M_{f2}, M_{f3}, and M_{f4}) by the primary winding (feeding loop). With the use of Kirchhoff's law, the circuit equations, which include the effects of the self and mutual partial inductances, can be

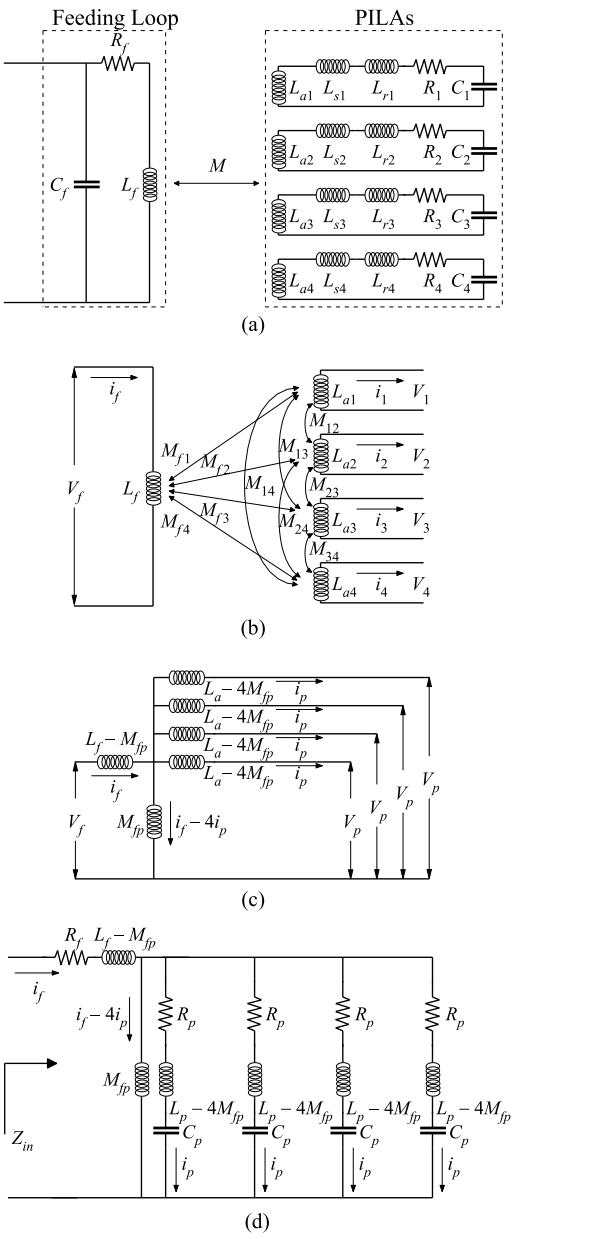

Fig. 10. Development of the equivalent circuit model. (a) General circuit model. (b) Simplified circuit model. (c) T-type circuit model. (d) Final circuit model.

derived as follows:

$$V_f = L_f\frac{di_f}{dt} - M_{f1}\frac{di_1}{dt} - M_{f2}\frac{di_2}{dt} - M_{f3}\frac{di_3}{dt} - M_{f4}\frac{di_4}{dt} \tag{9}$$

$$V_1 = -M_{f1}\frac{di_f}{dt} + L_{a1}\frac{di_1}{dt} + M_{12}\frac{di_2}{dt} + M_{13}\frac{di_3}{dt} + M_{14}\frac{di_4}{dt} \tag{10}$$

$$V_2 = -M_{f2}\frac{di_f}{dt} + M_{12}\frac{di_1}{dt} + L_{a2}\frac{di_2}{dt} + M_{23}\frac{di_3}{dt} + M_{24}\frac{di_4}{dt} \tag{11}$$

$$V_3 = -M_{f3}\frac{di_f}{dt} + M_{13}\frac{di_1}{dt} + M_{23}\frac{di_2}{dt} + L_{a3}\frac{di_3}{dt} + M_{34}\frac{di_4}{dt} \tag{12}$$

$$V_4 = -M_{f4}\frac{di_f}{dt} + M_{14}\frac{di_1}{dt} + M_{24}\frac{di_2}{dt} + M_{34}\frac{di_3}{dt} + L_{a4}\frac{di_4}{dt}. \tag{13}$$

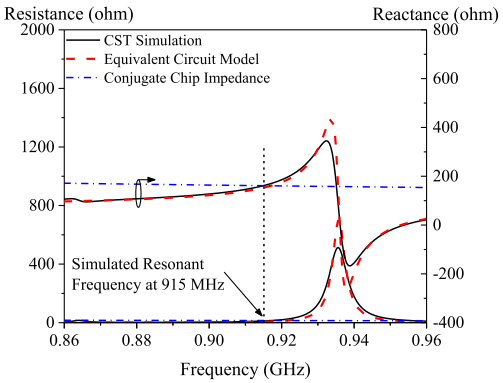

Fig. 11. Simulated and modeled input impedances of the tag antenna ($R_f = 0.139\ \Omega$, $L_f = 14.967$ nH, $M_{fp} = 1.45$ nH, $R_p = 0.410\ \Omega$, $L_p = 15.469$ nH, and $C_p = 1.870$ pF).

Since all the PILAs are identical and geometrically orthogonal, the mutual couplings of the arc segments are negligible ($M_{12} = M_{13} = M_{14} = M_{23} = M_{24} = M_{34} = 0$). Hence, (9)–(13) can be further reduced and a T-type equivalent circuit can be drawn, as shown in Fig. 10(c), where

$$V_f = \left(L_f - M_{fp}\right)\frac{di_f}{dt} + M_{fp}\frac{d\left(i_f - 4i_p\right)}{dt} \tag{14}$$

$$V_p = -M_{fp}\frac{d\left(i_f - 4i_p\right)}{dt} + \left(L_a - 4M_{fp}\right)\frac{di_p}{dt} \tag{15}$$

where $M_{fp} = M_{f1} = M_{f2} = M_{f3} = M_{f4}$, $i_p = i_1 = i_2 = i_3 = i_4$, $L_a = L_{a1} = L_{a2} = L_{a3} = L_{a4}$, and $V_p = V_1 = V_2 = V_3 = V_4$. Finally, other lumped elements ($L_s = L_{s1} = L_{s2} = L_{s3} = L_{s4}$, $L_r = L_{r1} = L_{r2} = L_{r3} = L_{r4}$, $R_p = R_1 = R_2 = R_3 = R_4$, $C_p = C_1 = C_2 = C_3 = C_4$, and $L_p = L_r + L_a + L_s$) are also included to obtain the final equivalent circuit in Fig. 10(d). The input impedance of the proposed tag antenna Z_{in} can, therefore, be expressed as

$$Z_{in} = R_f + j\omega L_f + 4\left(\omega M_{fp}\right)^2\frac{R_p - j\alpha}{R_p^2 + \alpha^2} \tag{16}$$

where $\alpha = \omega L_p - 1/\omega C_p$. The mutual partial inductance is found to be $M_{fp} = 1.45$ nH. As can be deduced from (16), the feeding loop can directly affect the antenna impedance by introducing the additional lumped elements R_f and L_f.

Next, the modeled impedance curve is compared with its simulated counterpart in Fig. 11, where good agreement has been observed, showing that the equivalent circuit is reasonable. The conjugate impedance of the chip, as shown in the same figure, is also shown for visualizing the tag resonance. They are derived from the parallel lumped resistance ($R_c = 1.80$ kΩ) and capacitance ($C_c = 1.07$ pF), as given in the datasheet [19], by using the parallel-to-series circuit transformation. The tag resonant frequency is found to be 915 MHz. With reference to Fig. 11, the intersecting resistance and reactance are found to be 12.07 and 161.51 Ω, respectively. This indicates that good impedance matching between tag antenna and the microchip is achieved and the power transmission coefficient (τ) at resonance is close to one.

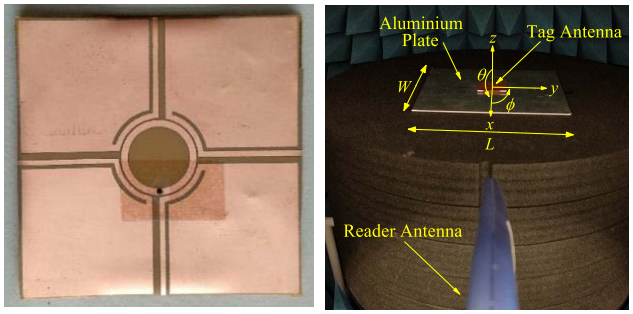

Fig. 12. (a) Top-down view of the fabricated tag antenna. (b) Tag antenna measurement setup in the anechoic chamber.

III. Results and Discussion

The prototype of the proposed tag antenna is fabricated and its read distance and realized gain are measured using the Voyantic Tagformance system, as shown in Fig. 12. Referring to Fig. 12(b), the tag is placed at the center of a piece of 20×20 cm^2 aluminium plate on a rotator inside the anechoic chamber. A linearly polarized reader antenna with a gain of 6 dBi is used and it is placed in the $+x$-direction of the tag with a fixed distance. This is because the proposed tag antenna has a maximum radiation in the azimuth plane. During the measurement, the reader antenna changes its transmitted power gradually until a backscattered power is received from the tag. This power is the threshold of the reader's transmitted power (P_t) which is sufficient to turn on the tag. Based on the obtained P_t, the tag sensitivity (P_{tag}) can then be calculated as $P_{tag} = P_t \times L_l$, where L_l is the measured forward-link loss. In the threshold measurement, the chip sensitivity can be related to P_{tag} by $P_c = P_{tag} \times G$, where $G = G_{tag} \times \tau$. Both P_{tag} and G are derived using Friis transmission equation [29]. After rearranging the terms, G can be expressed as $G = P_c/P_{tag} = P_c/(L_l \times P_t)$.

The simulated and measured realized gains as well as the measured tag sensitivity are plotted in Fig. 13. Referring to the same figure, the resonant frequency is measured to be 910 MHz with a realized gain of -6.71 dBi, which is slightly deviated from the simulated result (-5.17 dBi) at 915 MHz. The discrepancy is not unusual as microchip tends to have a larger fabrication tolerance. The tag antenna is found to have achieved the best sensitivity of -11.10 dBm at resonance.

The read distances of the proposed tag antenna are measured in different cut-planes in order to study its radiation properties. With reference to Fig. 12(b), a reader antenna, which is vertically polarized with respect to the tag antenna, is placed in the $+x$-direction of the tag with a fixed distance. Then, the tag's z-axis is aligned with the rotator's axis of rotation for obtaining the read pattern in the xy plane. For measurements in the xz and yz planes, the reader antenna is placed right above the tag antenna with a fixed distance, while allowing the tag antenna to rotate about its own y- and x-axes, respectively. Good omnidirectional radiation patterns have been obtained, as shown in Fig. 14. In the xy plane measurement, as shown in Fig. 14(a), a read distance of 5.9 m with even spatial coverage in the azimuth plane has been obtained. Fluctuation

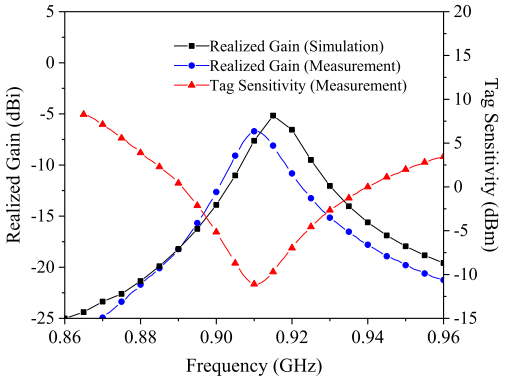

Fig. 13. Realized gain and tag sensitivity curves of the tag antenna when it is used on metal.

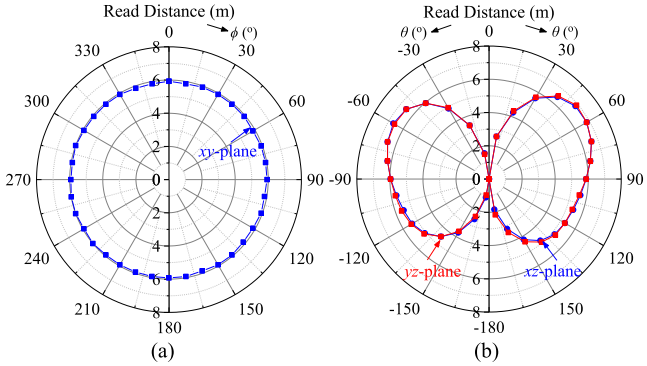

Fig. 14. Read patterns of the proposed tag antenna at the resonant frequency of 910 MHz. (a) *xy* plane. (b) *yz* and *xz* planes.

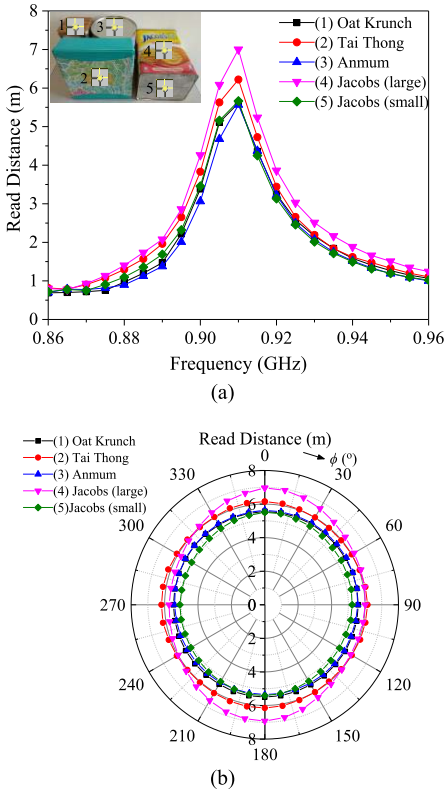

Fig. 15. (a) Read distances and (b) read patterns when the proposed tag antenna is tested on different household products.

in the read distance is found to be less than ∼0.1 m. With reference to Fig. 14(b), typical doughnut-shaped read patterns are observed in the *xz* and *yz* planes, with a null located in the direction normal to the tag antenna. It should be mentioned that the tag antenna is designed to be placed on the top surface of a metallic container, which is placed on a rack in the department store, for providing spatial coverage in the azimuth plane around it. In other words, the tag must be readable by the readers that are interrogating in all directions in its azimuth plane. For such application, an omnidirectional tag antenna that is able to work on metal surface is preferable.

The proposed tag antenna is also tested for several implementation scenarios with a couple of metallic household products randomly selected from a department store. As shown in Fig. 15(a), read distances for all the household products, which are measured from the *x*-axis direction, are all greater than 5.7 m. For all cases, it is noted that the tag's resonant frequency is very stable and it is not affected much by the backing metallic object, which is very desirable. With reference to Fig. 15(b), the fluctuation level in the omnidirectional patterns is found to be smaller than ∼1.3 m when the tag antenna is tested on different household products, showing that the omnidirectional characteristics are not affected much by the backing platform.

The proposed tag antenna is also compared with some other omnidirectional UHF tag antennas available in the literature. Referring to Table I, the tag in [30] is able to achieve the same read distance as ours with a much lower profile. However, this tag has a much poorer omnidirectional radiation characteristic, where the gain variation in the desired radiation plane is found to be 2.6 dB. Moreover, without the ground layer for isolation, the tag's resonance can get detuned when it is attached on different dielectric materials. Meanwhile, the tag with a much larger footprint (91 mm × 91 mm) in [31] has very limited applications although it has better performances in terms of bandwidth, stability of omnidirectional radiation pattern, and read distance. Different from the previously mentioned tags, the tag presented in [9] has good omnidirectional radiation characteristic (gain fluctuation of about 0.1 dB) and far read distance. However, this antenna structure, which is in an inlay form (the overall thickness is about 0.06 mm), requires a 2 mm spacer before it can be tagged on an object. Even so, the tag's resonant frequency was reported to have shifted by 20 MHz when it was tested on different dielectric constant materials. This could become a severe limitation when it is to be used for RFID applications. In [3], the tag that is close in size to ours is only able to achieve 2.8 m of read distance. Despite having a broader bandwidth, the tag loses its omnidirectivity when it is placed on metallic surface. This is because a planar dipole tends to have omnidirectional radiation pattern in its elevation plane and it can significantly vary with the electrical properties of the tagging object. Moreover, due to the boundary condition, all the above-mentioned tags, which are all horizontally polarized, are not able to provide spatial coverage in the azimuth plane when they are tagged on a metallic object.

TABLE I
COMPARISON OF DIFFERENT OMNIDIRECTIONAL UHF TAGS

References	This work	[3]	[9]	[30]	[31]
Tag Size (mm)	40.0 × 40.0 × 1.6	55.0 × 20.0 × 0.8	43.0 × 43.0 × 0.06	42.0 × 30.0 × 0.8	91.0 × 91.0 × 0.8
3 dB Bandwidth (MHz)	14	~36	22	27	124
Antenna Gain (dBi)	-5.08	-10.34	-0.30	NA	-1.90
E-Field Polarization	Vertically Polarized	Horizontally Polarized	Horizontally Polarized	Horizontally Polarized	Horizontally Polarized
Radiation Plane	Azimuth	Elevation	Azimuth	Elevation	Elevation
Gain Fluctuation (dB)	0.25	~1.50	0.10	2.60	~1.00
Max. Read Distance (m)	7.0 (4W EIRP)	~2.8 (4W EIRP)	9.5 (4W EIRP, with a 2 mm spacer)	2.6 (0.5W EIRP) ~7.4 (4W EIRP)	~10.0 (4W EIRP, on 2 mm glass sheet)
Application	On-metal	Non-metal	Non-metal	Non-metal	Glass

IV. CONCLUSION

A planar patch-type omnidirectional tag antenna has been proposed for on-metal applications. The directive radiation patterns of four PILAs, which are simultaneously excited by a circular loop, have been tactfully combined to design an on-metal tag that has good omnidirectional characteristics with low gain fluctuation in the azimuth plane. The loop exciter is found to be able to introduce additional reactance so that the antenna impedance can conjugate match with the chip impedance. The proposed tag antenna has compact size and low profile; it can be employed for practical applications that require sensing capability in all directions in the azimuth plane.

REFERENCES

[1] Y.-H. Lee, E.-H. Lim, F.-L. Bong, and B.-K. Chung, "Compact folded C-shaped antenna for metal-mountable UHF RFID applications," *IEEE Trans. Antennas Propag.*, vol. 67, no. 2, pp. 765–773, Feb. 2019.

[2] J.-P. Chen and P. Hsu, "A compact strip dipole coupled split-ring resonator antenna for RFID tags," *IEEE Trans. Antennas Propag.*, vol. 61, no. 11, pp. 5372–5376, Nov. 2013.

[3] Y. J. Zhang, D. Wang, and M. S. Tong, "An adjustable quarter-wavelength meandered dipole antenna with slotted ground for metallically and airily mounted RFID tag," *IEEE Trans. Antennas Propag.*, vol. 65, no. 6, pp. 2890–2898, Jun. 2017.

[4] F.-L. Bong, E.-H. Lim, and F.-L. Lo, "Compact folded dipole with embedded matching loop for universal tag applications," *IEEE Trans. Antennas Propag.*, vol. 65, no. 5, pp. 2173–2181, May 2017.

[5] A. E. Abdulhadi and R. Abhari, "Design and experimental evaluation of miniaturized monopole UHF RFID tag antennas," *IEEE Antennas Wireless Propag. Lett.*, vol. 11, pp. 248–251, Feb. 2012.

[6] K.-L. Wong, S.-W. Su, and C.-L. Tang, "Broadband omnidirectional metal-plate monopole antenna," *IEEE Trans. Antennas Propag.*, vol. 53, no. 1, pp. 581–583, Jan. 2005.

[7] X. Cai and K. Sarabandi, "A compact broadband horizontally polarized omnidirectional antenna using planar folded dipole elements," *IEEE Trans. Antennas Propag.*, vol. 64, no. 2, pp. 414–422, Feb. 2016.

[8] C.-C. Lin, L.-C. Kuo, and H.-R. Chuang, "A horizontally polarized omnidirectional printed antenna for WLAN applications," *IEEE Trans. Antennas Propag.*, vol. 54, no. 11, pp. 3551–3556, Nov. 2006.

[9] Q. Liu, Y. Yu, and S. He, "Capacitively loaded, inductively coupled fed loop antenna with an omnidirectional radiation pattern for UHF RFID tags," *IEEE Antennas Wireless Propag. Lett.*, vol. 12, pp. 1161–1164, Sep. 2013.

[10] D. Liao and K. Sarabandi, "Terminal-to-terminal hybrid full-wave simulation of low-profile, electrically-small, near-ground antennas," *IEEE Trans. Antennas Propag.*, vol. 56, no. 3, pp. 806–814, Mar. 2008.

[11] Y. Liu, X. Li, L. Yang, and Y. Liu, "A dual-polarized dual-band antenna with omni-directional radiation patterns," *IEEE Trans. Antennas Propag.*, vol. 65, no. 8, pp. 4259–4262, Aug. 2017.

[12] B.-C. Park and J.-H. Lee, "Omnidirectional circularly polarized antenna utilizing zeroth-order resonance of epsilon negative transmission line," *IEEE Trans. Antennas Propag.*, vol. 59, no. 7, pp. 2717–2721, Jul. 2011.

[13] Y. M. Pan and K. W. Leung, "Wideband omnidirectional circularly polarized dielectric resonator antenna with parasitic strips," *IEEE Trans. Antennas Propag.*, vol. 60, no. 6, pp. 2992–2997, Jun. 2012.

[14] W. W. Li and K. W. Leung, "Omnidirectional circularly polarized dielectric resonator antenna with top-loaded alford loop for pattern diversity design," *IEEE Trans. Antennas Propag.*, vol. 61, no. 8, pp. 4246–4256, Aug. 2013.

[15] W.-H. Ng, E.-H. Lim, F.-L. Bong, and B.-K. Chung, "Compact planar inverted-S antenna with embedded tuning arm for on-metal UHF RFID tag design," *IEEE Trans. Antennas Propag.*, vol. 67, no. 6, pp. 4247–4252, Jun. 2019.

[16] *ECCOSTOCK PP*. Accessed: Oct. 2017. [Online]. Available: http://www.eccosorb.com/Collateral/Documents/English-US/PP.pdf

[17] T. Milligan, V. Schejbal, and V. Kovarik, "A method of cross-polarization reduction," *IEEE Antennas Propag. Mag.*, vol. 48, no. 5, pp. 108–111, Oct. 2006.

[18] Y.-H. Lee, E.-H. Lim, F.-L. Bong, and B.-K. Chung, "Folded antipodal dipole for metal-mountable UHF tag design," *IEEE Trans. Antennas Propag.*, vol. 66, no. 11, pp. 5698–5705, Nov. 2018.

[19] *Monza 5 Tag Chip Datasheet, Rev 0.9*, document IPJ-W1610, Aug. 2012.

[20] C. Pfeiffer, "Fundamental efficiency limits for small metallic antennas," *IEEE Trans. Antennas Propag.*, vol. 65, no. 4, pp. 1642–1650, Apr. 2017.

[21] Y. Huang and K. Boyle, "RFID antennas," in *Antennas: From Theory to Practice*. Chichester, U.K.: Wiley, 2008, ch. 8, sec. 4, pp. 339–351.

[22] B. A. Austin, A. Boswell, and M. A. Perks, "Loss mechanisms in the electrically small loop antenna [antenna designer's notebook]," *IEEE Antennas Propag. Mag.*, vol. 56, no. 4, pp. 142–147, Aug. 2014.

[23] C. R. Paul, "Self inductance of a current loop from Faraday's law of induction," in *Inductance: Loop and Partial*. Hoboken, NJ, USA: Wiley, 2010, ch. 4, sec. 1, pp. 117–133.

[24] S. Caniggia and F. Maradei, "Appendix A—Formulae for partial inductance calculation," in *Signal Integrity and Radiated Emission of High-Speed Digital Systems*. Hoboken, NJ, USA: Wiley, 2009, pp. 481–486.

[25] R. Simons, "Coplanar waveguide applications," in *Coplanar Waveguide Circuits, Components, and Systems*. New York, NY, USA: Wiley, 2001, ch. 12, pp. 384–433.

[26] *The AC Resistance of Rectangular Conductors*. Accessed: Oct. 2017. [Online]. Available: http://g3rbj.co.uk/wp-content/uploads/2017/06/The-ac-Resistance-of-Rectangular-Conductors-Payne-Issue-3.pdf

[27] R. King, C. Harrison, and D. Denton, "Transmission-line missile antennas," *IRE Trans. Antennas Propag.*, vol. 8, no. 1, pp. 88–90, Jan. 1960.

[28] C. Sun, N. H. Kutkut, D. W. Novotny, and D. M. Divan, "General equivalent circuit of a multi-winding co-axial winding transformer," in *Proc. IEEE Ind. Appl. Conf. 30th IAS Annu. Meeting (IAS)*, Orlando, FL, USA, Oct. 1995, pp. 2507–2514.

[29] R. Colella, L. Catarinucci, P. Coppola, and L. Tarricone, "Measurement platform for electromagnetic characterization and performance evaluation of UHF RFID tags," *IEEE Trans. Instrum. Meas.*, vol. 65, no. 4, pp. 905–914, Apr. 2016.

[30] S.-L. Chen, K.-H. Lin, and R. Mittra, "Miniature and near-3D omnidirectional radiation pattern RFID tag antenna design," *Electron. Lett.*, vol. 45, no. 18, pp. 923–924, Aug. 2009.

[31] Y.-F. Lin, S.-A. Yeh, H.-M. Chen, and S.-W. Chang, "Design of an omnidirectional polarized RFID tag antenna for safety glass applications," *IEEE Trans. Antennas Propag.*, vol. 60, no. 10, pp. 4530–4537, Oct. 2012.